Assessing electrical degradation of microelectrode encapsulations with accelerated-life testing

Ben Rees[1] and Mohammad Mundiwala[2]

[1] Combustion Diagnostics Laboratory
[2] Reliability Engineering and Informatics Laboratory

Keywords: Charge storage capacity, electronics, mems

Abstract. Precise evaluation of soft neural microelectrode performance and safety is crucial for successful implementation. In this work, we use electrochemical impedance spectroscopy (EIS), cyclic voltammetry (CV), and voltage transient (VT) measurements to evaluate the degradation of the electrode encapsulation. EIS revealed a 47% decrease in impedance at 1 kHz, after x days. The average cathodic charge storage capacity (CSC_c) decreased by 0.16 mC cm^{-2} (or -19%) and the average charge injection capacity (CIC) increased by 8.13 mC cm^{-2} (or 1490 %); these results are attributed to indicating artifacts of experimental measurement rather than true degradation like delamination. Finally, an Equivalent Circuit Model (ECM) was fit using the EIS data to discriminate the impact of individual elements in the stimulation process. Nuance in the presented results and future improvements for the methods are discussed.

1 Introduction

Many modern solutions to Parkinson's disease, epilepsy, spinal cord injury and depression are built on our ability to communicate with the nervous system. Among many design requirements, neural interfacing devices must effectively and safely stimulate and record electrical impulses from neural tissue. Microelectrodes require special characterization methods because their performance must span a wide range of high-charge signals without incurring damage to the surrounding tissue or the electrode itself, and must do so over long periods of time. This report provides a comprehensive characterization of the electrode channels of an electrode-encapsulation unit in order to evaluate the safety and efficacy of a design one the day of fabrication and after accelerated life testing, mimicking the potential wear from an in-vivo environment.

The key structure of the neural interface is the formation of the electrical double layer, which is the capacitor-like attraction and repulsion of electrolyte ions at the electrode surface which spontaneously forms and transfers charge without chemical reactions occurring. This capacitive charge transfer is foundational to effective neural recording as it allows for the non-destructive sensing of minute voltage fluctuations present in neural activity. Low impedance and a phase angle approaching -90° as probed by electrochemical impedance spectroscopy (EIS) demonstrate a high-quality recording interface.

Faradaic charge transfer are ideal for effective stimulation and can be measured by the charge storage capacity (CSC) calculated from cyclic voltammetry (CV). Large CSC indicates a sizable charge reservoir which allows for sufficient charge injection that still remains within safe interface voltage potentials.The maximum charge able to be injected while remaining within the "water

21 September 2025

window" [1] is known as the charge injection capacity (CIC) and is analyzed via the voltage transient (VT) probed with alternating current application.

By comparing the EIS, CSC, and CIC results from day 1 and day x, the performance reliability of the electrode- encapsulation unit can be assessed.

2 Data and Methods

Flexible electrodes were implanted into a flexible encapsulation via metal deposition and photolithography. The resulting electrode heads (connection sites) may be seen in Figure 1.

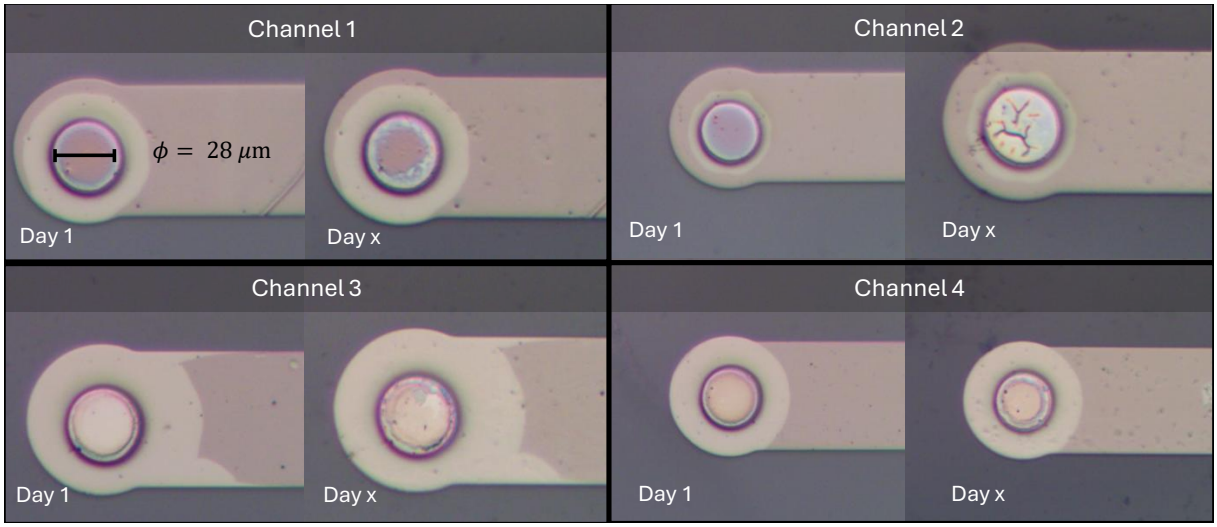

Figure 1: Side by side comparison of electrode channel heads on day 1 (left) and day x (right).

The electrode channel connection site was produced with a diameter of 28 μm. The entire encapsulation was then suspended in a simulated neural electrolyte bath, with the electrode channel head connected to a power unit and a reference signal connected to the electrolyte bath nearby to the encapsulation. Electrical signals were then passed through the electrode-encapsulation unit to evaluate various performance metrics as is described in the sections below.

2.1 Electrochemical Impedance Spectroscopy

Electrochemical impedance spectroscopy, or EIS, is used to measure the electric impedance and phase angle frequency dependence across the electrode [2]. We span from 0.1 Hz to 100 kHz with a sinusoidal amplitude of 50 mV (small enough to assume linearity) and an initial quiet time of 2 seconds. This testing is done across 4 of the 5 electrodes in the tested unit. The resulting impedance magnitude and phase were then plotted in a Bode plot as is found in Figure 3.

The change in impedance at 1 kHz is especially important because electrodes with particularly low impedance at 1 kHz will have a favorable signal to noise ratio (SNR), detecting the more quiet action potentials from within the general electrical background noise of the brain and electrode itself. Measuring this impedance is therefore necessary after an accelerated life test to ensure functional stability over time.

2.2 Cyclic Voltammetry

Cyclic voltammetry (CV) is an electrode measurement where the potential of a test electrode is swept cyclically at a constant rate between -0.6 V and 0.8 V while the current flowing between the test electrode and a counter electrode is recorded [2]. In this report we characterize the electrodes by their cathodal charge storage capacity ($\mathrm{CSC_c}$). The $\mathrm{CSC_c}$ is calculated using

$$\mathrm{CSC_c} = \frac{1}{\nu A} \int_{V_{min}}^{V_{max}} i(V)\, dV \tag{1}$$

where ν is the sweep rate (0.1 V/s), A is the area of the electrode calculated based on the electrode interface diameter, i is the measured current, and V_{min} and V_{max} are the potentials just within the water electrolysis window taken as - 0.6 V and 0.8 V, respectively. The CSC_c represents the total reservoir capacity of the electrode-encapsulation unit, with larger values indicating a higher capacity to safely inject large charges and in turn more thorough signal generation. The values were calculated from the final of 4 total loops, allowing the system to stabilize.

The resulting current was plotted against the applied potential for the four channels and may be viewed in Figure 4. The cathodic charge storage capacity was found by integrating the area graphically bounded by $i = 0$ and the internal area of the current versus applied potential curve and dividing by the scan rate and the electrode channel-head area.

2.3 Voltage Transients

Voltage transient, or VT, measurements are used to estimate the charge injection capacity, and are performed via a current-controlled stimulation pulse [2]. The transients are analyzed to determine the maximum polarization across the electrode-electrolyte interface. The voltage transient is defined by

$$\Delta V = i_c R_i + \eta_c + \eta_a + \Delta E, \tag{2}$$

where i_c is the current applied, R_s is the solution resistance, η_c and η_a are the cathodic and anodic overpotential, an ΔE is the polarization value. In this work, we take the empirical ΔE as

$$\Delta E = V_{\text{baseline}} - V_{\text{peak,cathodic}}, \tag{3}$$

and is calculated directly from transient data. Note that calculating ΔE this way includes both solution-resistance drop and electrode polarization; still, this estimate can be useful to assess safe operation within a desired window (i.e., water window).

2.4 Remaining useful life

We estimate the equivalent lifetime at 37°C using the Arrhenius equation

$$Q_{10} = \frac{R_2}{R_1}^{\frac{10}{T_2 - T_1}} \tag{4}$$

with Q_{10} values off 1.5, 2.0, and 2.5. The accelerated aging tests are conducted in 87° C chamber for four weeks. In order to determine the acceleration factor of this aging test, AF we assess the ratio of the aging rates, R_2 and R_1. Rearranging Eq. (4), we define AF as

$$AF = Q_{10}^{\frac{T_2 - T_1}{10}}. \tag{5}$$

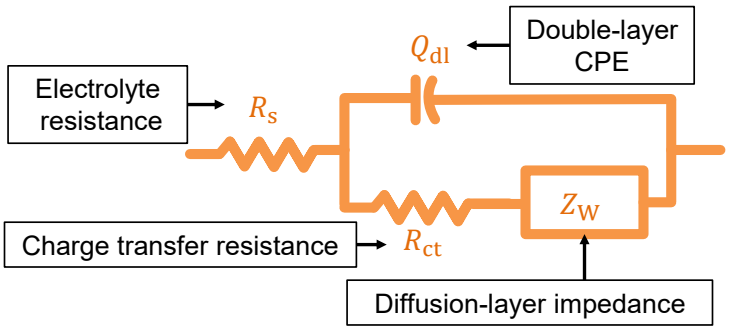

Figure 2: The ECM model used to in this work

2.5 Equivalent Circuit Modeling

EIS data can be difficult to interpret by using first principles. It is useful to understand the impedance of the electrode-encapsulation as a function of individual impedance arises from different elements in the interaction. The electrical impedance from charge-transfer phenomena across the encapsulation interface is often modeled with a resistor while the double-layer build up is more closely modeled as a capacitor. By representing the system with an an accurate ECM can offer physical interpretations to EIS response. For example, after accelerated life testing, we may visually see delamination (with macro imaging); in the ECM model, the same phenomenon may manifest as a large increase in the charge-transfer resistance. We note that fitting an appropriate ECM is non-trivial since simple models will be easy to interpret but will struggle to perfectly match the data while highly-complex models will be able to match the experimental data but with a trade-off in interpretability.

3 Results and Discussions

3.1 EIS, CV, and VT Results

Average impedance for the four tested channels at 1 kHz was found to decrease from $5.64 \times 10^5\ \Omega$ to $3.02 \times 10^5\ \Omega$, with similar behavior in all electrode channels, which is a relatively high impedance compared to more ideal levels cited at 50-100 kΩ [2]. The frequency-dependent phase and impedance response plot shows much less channel-to-channel variation after on day x than on day 1. shows a larger discrepancy between channels, potentially indicating inconsistent encapsulation quality, non-uniform surface coating, or surface contamination on the electrodes. Phase response decreasing to -110° at high frequencies suggests the influence of inductive artifacts from the wiring in the test setup as the impedance from the electrode-electrolyte interface becomes less dominant. We see this in both the day 1 and day x responses.

The CV results are plotted in Figure 4 and the calculated CSC_c for each electrode is given in Table 1. The charge storage capacity is adequate for neural stimulation in all channels, but is abnormally high in the third channel. Similar to the EIS phase response results, this anomalously high value along with the distinct connection site appearance able to be seen in Figure 1 suggests inconsistent encapsulation quality, inconsistent surface coating, or surface contamination, all of which could lead to the high value of CSC_c recorded.

More useful than the CSC_c, however, is the charge injection capacity (CIC), as measured from VT, as it simulates stimulation transients and measures the true safe limit of the device to inject charge. The applied current profile is shown in the bottom of Figure 5 and the resulting voltage

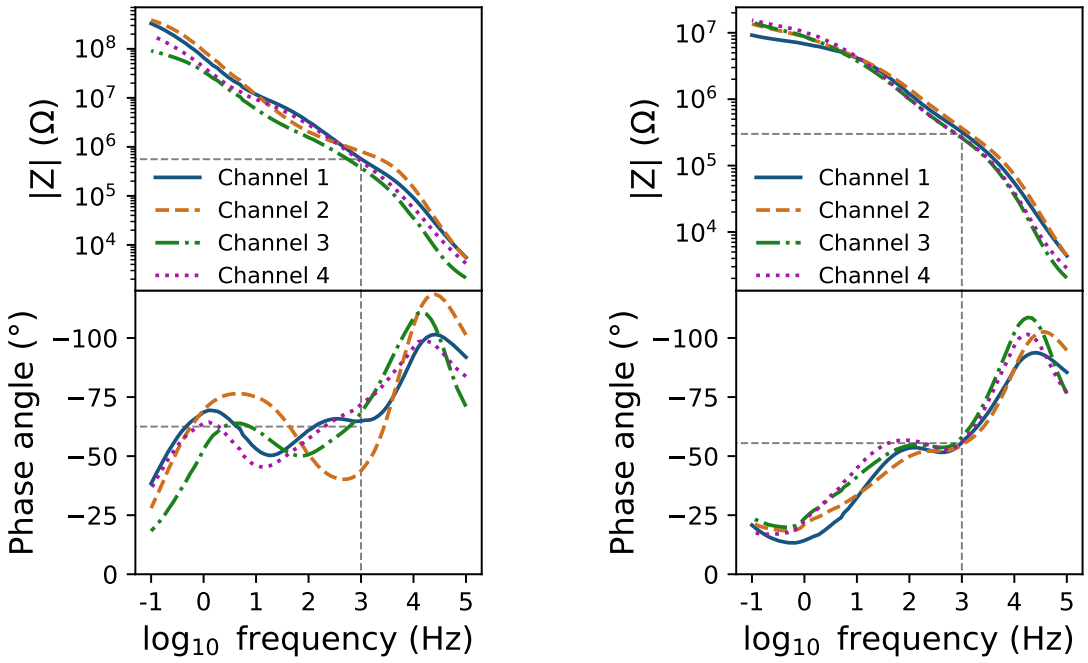

(a) Day 1

(b) Day x

Figure 3: Comparing EIS measurements on day 1 and day x for four channel heads on the electrode. On day 1 (left), at 1 kHz, the mean impedance and phase angle are $5.65 \times 10^5\ \Omega$ and $-62.5°$ and on day x the mean impedance and phase angle are $3.0 \times 10^5\ \Omega$ and $-56.1°$.

Channel	Δ_{CIC} ($\frac{\text{mC}}{\text{cm}^2}$)	Γ_{CIC}	Δ_{CSC} ($\frac{\text{mC}}{\text{cm}^2}$)	Γ_{CSC}
1	10.9	22.4	-0.146	0.81
2	7.9	22.1	-0.13	0.83
3	8.5	6.8	-0.26	0.73
4	5.2	8.2	-0.10	0.88

Table 1: **CV and VT results**. Charge injection capacity and charge storage capacity are derived from voltage transient data and cyclic voltammetry integration, respectively. Δ represents the difference and Γ represents the ratio factor.

transients may be seen above it.

The mean polarization ΔE across the four electrodes decreased from 0.971 ± 0.034 V on day 1 to 0.757 ± 0.027 V on day x. It is also readily apparent that the baseline-voltages from the results on day 1 and day x are not significantly different. On day 1 the mean baseline voltage is 0.383 V meanwhile, on day x, it is just 0.173 V. Once again, this is more indicative of the the experimental variation (environment, measurement, etc) than the degradation of the electrode itself. We discuss this point in more detail in Section 4.

From Figure 5 we can see the fast drop during the cathodic step and the fast rise during the anodic step, as expected. The peak cathodic voltage remains within the acceptable water window across all electrodes which is a good sign. The variance across electrodes is minimal and suggests that contact surfaces are consistent. Under the tested current pulses, the electrode behavior is classified as reversible since the potential returns to the same baseline after each cycle and because the charge and discharge plots (Figure 5) is capacitive in nature.

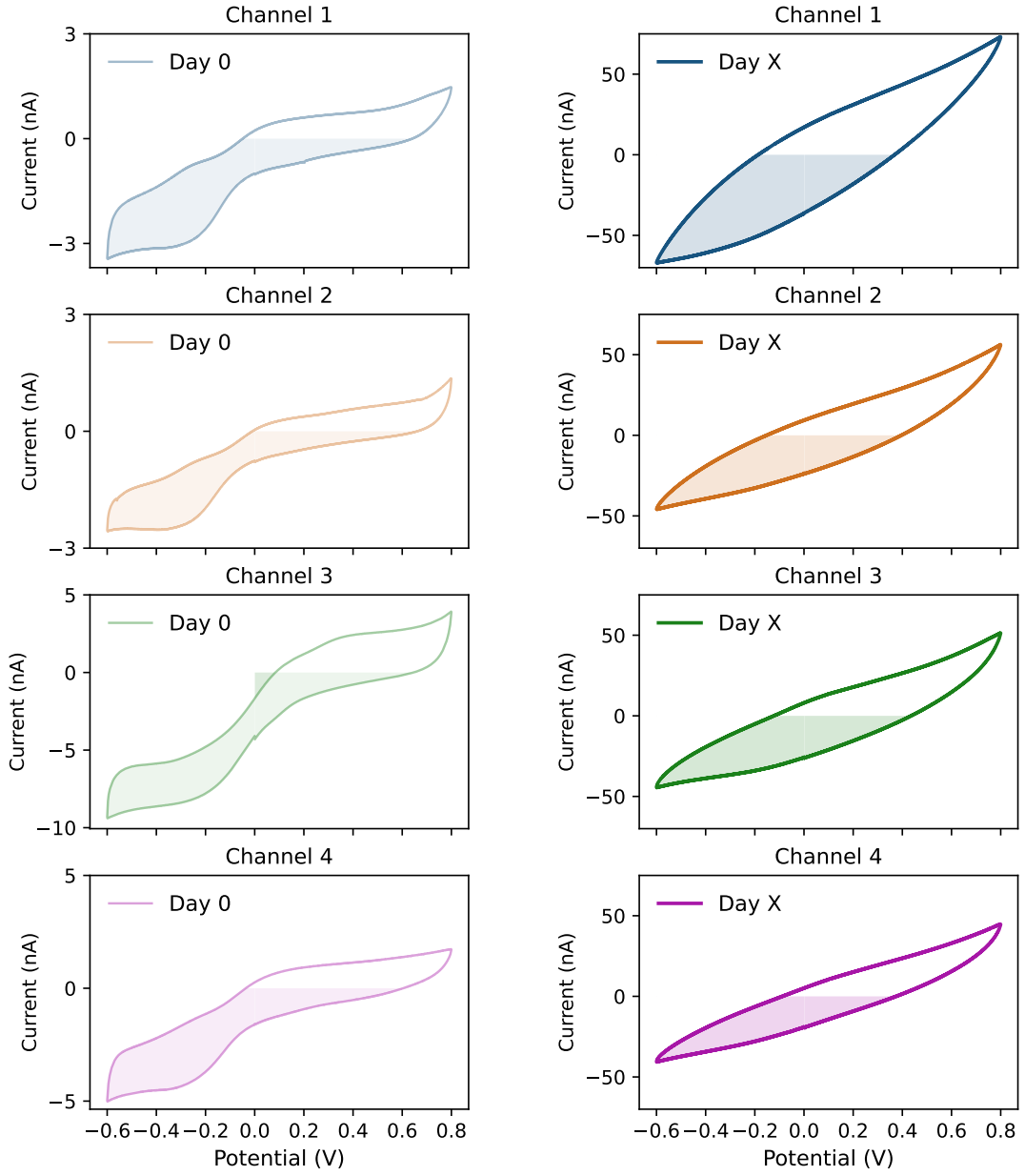

(a) Day 1 (b) Day x

Figure 4: Cyclic voltammetry plot for the final loop that was recorded; shaded area indicates the cathodic region used to calculate the charge storage. Note that day x subplots are an order of magnitude larger scale despite similar looking shape sizes.

3.2 Lifetime projection

Using Q_{10} values of 1.5, 2, and 2.5 in Eq. (5), we can estimate that the aging done was equivalent to about 23, 79, and 206 weeks at 37°C. As shown by the results in the prior section, impedance, CIC and CSC were impacted beyond functionality, allowing us to expect the electrode to withstand many months to years of operation at body temperature, before any critical failure. The results of this experiment would be more complete if more frequent EIS measurements were used up until the electrode showed critical failure.

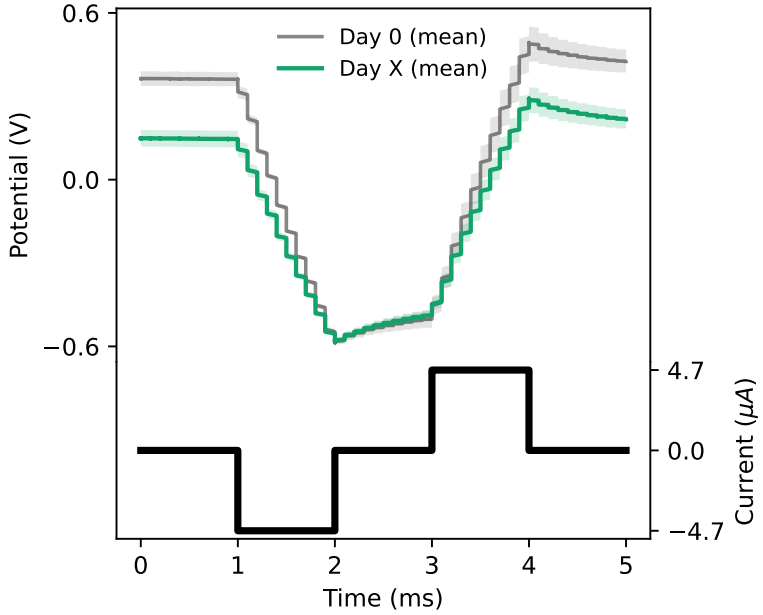

Figure 5: Voltage transient of a single cycle taken as a mean of the 4 channels. Note that the input current of only channel 1 on day 1 is shown; they are not all identical.

3.3 ECM Results

Prior to fitting the EIS measurements to the ECM, [3] suggests first verifying that the measured signal has the capacity to be modeled. The Linear Kramers-Kronig test helps to validate that the measured impedance data obeys the four following rules: (1) Causality, (2) Linearity, (3) Stability, and (4) Time-invariance. For brevity, the details of this assumptions can be found in [3] and implemented in 'pyEIS' open-source repository [4].

We fit the data to Kramers-Kronig test and plot a representative sample in Figure 6. It can be seen that the real and imaginary impedance $\Delta Z'$ and $\Delta Z''$, respectively, have residuals that generally stay within $\pm 3\%$, indicating a model-able measurement set. This result remained true while using 24, 48, and 150 KK elements. Note, that the included figure represents a single channel (channel 3) from Day 1, but all 4 channels from Day 1 and x present similar residual plots or better.

An extended-Randles circuit was used to model the EIS electrode-encapsulation system in this work, shown by Figure 2.

We show the average (across channels) ECM parameter values with a the bar chart in Figure 7 to show the aggregated differences in parameter values for the electrode channel heads.

The ECM fits showed that Q_{dl} roughly doubled, indicating greater ionic access, while R_{ct} dropped, potentially indicating the appearance of a small faradaic pathway. These shifts likely reflect minor surface changes (roughening, small defects) rather than anything significant like corrosion.

For delamination, we would expect that R_{ct}, the charge-transfer resistance, to increase due to the increased effective surface area of the electrode. Counter intuitively, the charge-transfer resistance decrease by almost 2 orders of magnitude. This, far more likely indicates that the day 1 EIS measurements were erroneous. It is challenging to identify if day 1 or day x measurements were misaligned (or potentially both) since there is no expected parameter values for the given electrode-electrolyte-encapsulation system. From examples in the literature, we feel confident that these parameters are generally remained in realistic ranges, and the parameters did not

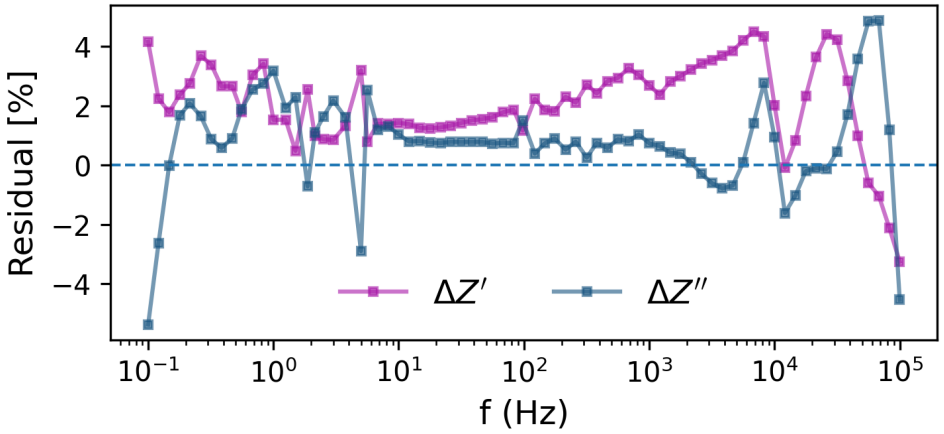

Figure 6: Plotting the residuals of true and predicted impedance values for real ($\Delta Z'$) and imaginary ($\Delta Z''$).

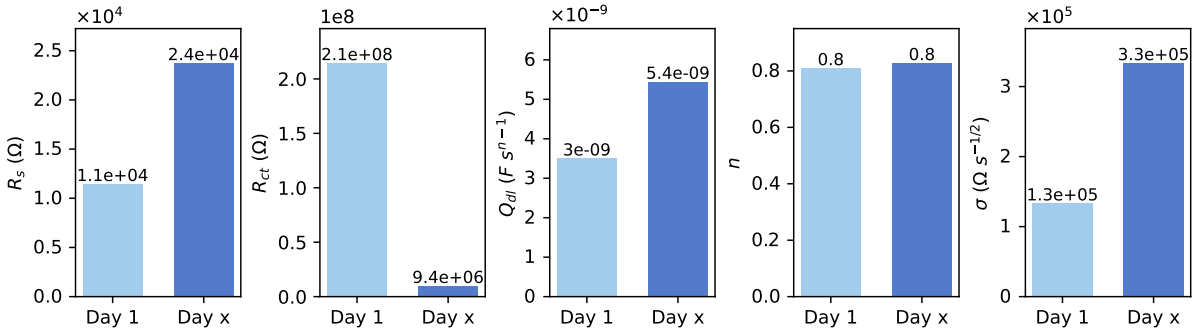

Figure 7: ECM parameter values on day 1 and day x

falsely converge (fit to their user-defined, upper or lower bounds).

4 Discussion and conclusion

In this report we used the framework shown in lab 1 to characterize microelectrodes in order to assess performance changes after conducting accelerated aging tests. Based on EIS, CV, and VT results, we show that the device can safely inject charges appropriate for neural stimulation within a safe voltage window and that charge transfer is reversible on both day 1 and day x.

Known failure modes for implanted electrodes include polymer cracking or delamination, moisture ingress leading to hydrolysis and increased interfacial impedance. Higher temperature is intended to accelerate processed like diffusion, chemical reactions, material fatigue, etc., commonly associated with the aforementioned failure modes. We found that the impedance actually decreased and all channels remained electrically viable and stable; additionally, the CV curves did not exhibit new faradaic peaks indicative of corrosion. Visually, the electrodes did not show obvious delamination or material loss after the test (no peeling or exposed metal corrosion spots in Fig. 1). This suggests that the encapsulation and electrode materials could withstand the accelerated aging quite well or, more likely, that the aging was not performed for long enough.

The slight drop in CSC could be interpreted as early-stage degradation. For example, the formation of micro cracks may be starting, but they have not yet progressed to the point of causing critical failure. Based on this, lifetime projection analysis weakly indicated that the

device could operate on the order of a few years without serious performance loss, since we did not induce mechanical stresses or other environmental effects. The CV and VT metrics presented a mixed result (CSC slightly decreased while CIC dramatically increased). We interpret this as largely stemming from measurement nuances and minor surface changes rather than any fundamental improvement. The ECM analysis supports this, indicating a small increase in capacitive behavior and doubled diffusion-based impedance. An obvious weakness to this study is the two-point time frame which limits the conclusiveness of any results. Future work should incorporate more intermediate testing and multiple samples to capture the full progression of aging and to ensure that these results are representative.

Appendix

The CIC and CSC values used to calculate the values in Table 1 are included below in Tables 2 and 3.

Channel	**CIC** ($\frac{\text{mC}}{\text{cm}^2}$)	**CSC**$_c$($\frac{\text{mC}}{\text{cm}^2}$)
1	0.763	0.510
2	0.747	0.376
3	0.974	1.449
4	0.812	0.728

Table 2: **DAY 1** CV and VT results. Charge injection capacity and charge storage capacity derived from voltage transient data and cyclic voltammetry integration, respectively.

Channel	**CIC** ($\frac{\text{mC}}{\text{cm}^2}$)	**CSC**$_c$($\frac{\text{mC}}{\text{cm}^2}$)
1	0.617	11.43
2	0.617	8.31
3	0.715	9.90
4	0.715	5.96

Table 3: **DAY x** CV and VT results. Charge injection capacity and charge storage capacity derived from voltage transient data and cyclic voltammetry integration, respectively.

Availability of data and code

Our code is available at the following URL: https://github.com/mohammadmundiwala/Flexible-Electronics/tree/main/lab-5.

References

[1] Kyungjin Kim. Introduction to flexible and stretchable electronics. Lecture notes for ME 5895, 2025. Accessed: 2025-09-15.

[2] Stuart F Cogan. Neural stimulation and recording electrodes. *Annu. Rev. Biomed. Eng.*, 10(1):275–309, 2008.

[3] Bernard A Boukamp. A linear kronig-kramers transform test for immittance data validation. *Journal of the electrochemical society*, 142(6):1885, 1995.

[4] Kristian B Knudsen. Pyeis: a python-based electrochemical impedance spectroscopy simulator and analyzer. *Zenodo*, 2021.